Int. J. Solids Structures Vol. 27, No. 14, pp. 1757–1771, 1991
Printed in Great Britain.

0020–7683/91 $3.00 + .00
© 1991 Pergamon Press plc

EFFECT OF A VISCOELASTIC INTERFACE ON THE TRANSVERSE BEHAVIOR OF FIBER-REINFORCED COMPOSITES

M. GOSZ, B. MORAN and J. D. ACHENBACH
Center for Quality Engineering and Failure Prevention, Northwestern University, Evanston, IL 60208-3020, U.S.A.

(*Received* 2 *April* 1990; *in revised form* 9 *July* 1990)

Abstract—In this paper we investigate the effect of a viscoelastic interfacial zone on the mechanical behavior of a transversely loaded fiber-reinforced composite. A simple linearly viscoelastic model is used to characterize the stiffness and viscosity of the interface separating the fibers and the matrix. The mechanical response is obtained using the finite element method and calculations are carried out for a unit cell in a periodic array of hexagonally packed fibers. An approximate representation of the time-dependent macroscopic behavior of the composite is derived analytically and compared with the numerical results. From a micromechanical perspective, the influence of interfacial stress relaxation on the stress fields in the matrix material contiguous to the interface is also examined.

1. INTRODUCTION

Since the advent of the modern fiber-reinforced composite, the determination of the mechanical properties of these materials has become of significant practical importance. Unlike the axial strength and stiffness properties which are primarily governed by the axial properties of the fiber, the behavior of a fiber-reinforced composite in the transverse direction is dominated by a relatively low stiffness matrix material and the nature of the bond between the fiber and matrix phases. This may place severe limitations on the overall performance of the composite and thus it is desirable to accurately characterize the transverse properties.

In most analytical and numerical work, investigators have assumed a perfect bond between the fibers and the matrix material which is modeled by continuity of interfacial tractions and displacements. In reality, however, a more complex state exists between the fiber and matrix constituents, and the assumption of perfect bonding may not be suitable in the presence of a thin interfacial zone which connects the two phases (e.g. fiber coating or intermolecular bonding). In this analysis it is assumed that the bond between the fibers and the matrix is effected across an infinitesimally thin interfacial zone which supports a traction field with both normal and tangential components. Continuity of tractions is assumed across the interface; however, displacements may be discontinuous from fiber to matrix due to the presence of the interfacial zone in between. Such a model, assuming a linear relationship between the displacement jumps across the interface and the conjugate tractions, is employed by Aboudi (1987), Steif and Hoysan (1987), Achenbach and Zhu (1989a,b) and Hashin (1990). Needleman (1987) utilizes this model to simulate the bond between rigid spherical inclusions embedded in an isotropically hardening elastic–viscoplastic matrix and considers a more general interfacial constitutive relation.

In implementing the above-mentioned interface model, care must be taken in order to avoid an unrealistic interpenetration of the matrix and fiber phases which can occur in local regions of compression. As will be seen later, the imposition of such a constraint significantly influences the transverse mechanical behavior of the composite with a relatively low stiffness interfacial zone.

In the present paper, the role of a viscoelastic interface on the transverse properties of a fiber-reinforced composite is considered from both a macroscopic and a microscopic perspective. The choice of a relatively simple linearly viscoelastic interface model allows us to derive an approximate representation for the transverse relaxation moduli of the composite with which to compare our numerical results. We note that this analytical model does not incorporate the aforementioned impenetrability constraint, and of primary interest

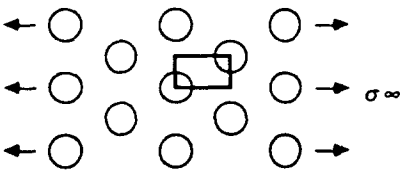

Fig. 1. Mid-CPD loading configuration for the hexagonal array composite.

is how well it compares with the numerical results over a range of interfacial stiffness parameters. In addition, the influence of interfacial stress relaxation on the stress fields in the matrix material contiguous to the interface is examined from a micromechanical viewpoint.

In the following section, the model which is chosen to represent the behavior of a unidirectional, fiber-reinforced composite is described and the boundary value problem is formulated. Discussed in Section 3 are implementational details of the finite element method, the numerical procedure employed in this analysis. In Section 4, the analytic model which approximates the transverse relaxation moduli of the fiber-reinforced composite is described and compared with the numerical results. In Section 5, a qualitative discussion is presented regarding the effect of interfacial stress relaxation on the resulting stress fields in the matrix material near the fiber/matrix interface. Finally, some concluding remarks are stated in Section 6.

2. FORMULATION OF THE BOUNDARY VALUE PROBLEM

A cross-sectional view of the model employed in this analysis is illustrated in Fig. 1. It is assumed that the fibers, all of equal radius, a, are periodically spaced in a regular hexagonal array and are embedded in an infinite matrix. Two loading directions are considered in this analysis, the closest packing direction (CPD) and the mid-closest packing direction (mid-CPD). The mid-CPD loading direction which bisects the angle formed by two closest packing directions is illustrated in Fig. 1.

Through arguments of symmetry, it is only necessary to analyze the rectangular region outlined in Fig. 1 and shown in detail in Fig. 2. Neglecting all rigid body motion, the point O, located at the origin of the Cartesian coordinate system shown in the figure, is considered fixed throughout the analysis. By imposing the appropriate boundary conditions on one half of this rectangular region, i.e. the trapezoid ABEF consisting of one quarter of a regular hexagon with sides of length b, the state of stress and strain for the entire model may be completely characterized.

2.1. *Boundary conditions*

The relevant boundary conditions for the case of CPD loading are given below. The corresponding expressions for the case of mid-CPD loading are obtained similarly, see e.g. Achenbach and Zhu (1989b). Referring again to Fig. 2, the loading direction is parallel to

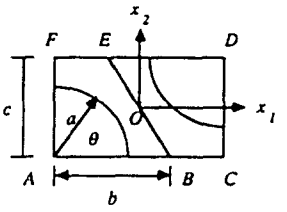

Fig. 2. Schematic of the representative cell of the hexagonal array composite.

Table 1. Elastic constants of the graphite epoxy material system considered.

	$E_A(GPa)$	ν_A	$E_T(GPa)$	ν_T	$G_A(GPa)$	$G_T(GPa)$	$K_T(GPa)$
Graphite fiber	232	0.279	15.0	0.490	24.0	5.03	15.0
Epoxy matrix	5.35	0.354	5.35	0.354	1.976	1.976	6.76

the x_2 axis of the Cartesian reference frame centered at O. Relative to this frame, the boundary conditions along the external boundaries AB, EF, and AF respectively are expressed as follows:

$$x_1 \in \left[-\frac{3b}{4}, \frac{b}{4}\right], \quad x_2 = -\frac{\sqrt{3}}{4}b,: \quad \sigma_{21} = 0, \quad u_2 = -\Delta_2 \tag{1}$$

$$x_1 \in \left[-\frac{3b}{4}, \frac{b}{4}\right], \quad x_2 = +\frac{\sqrt{3}}{4}b,: \quad \sigma_{21} = 0, \quad u_2 = +\Delta_2 \tag{2}$$

$$x_2 \in \left[-\frac{\sqrt{3}}{4}b, +\frac{\sqrt{3}}{4}b\right], \quad x_1 = -\frac{3b}{4},: \quad \sigma_{12} = 0, \quad u_1 = -\Delta_1 \tag{3}$$

where u_1 and u_2 are the displacement components in the x_1 and x_2 directions and Δ_2 is the magnitude of the prescribed displacement in the x_2 direction along AB and EF. The quantity Δ_1 is the magnitude of the unknown displacement in the x_1 direction along AF to be determined as part of the numerical solution. Along BE, the following displacement condition must hold:

$$u_1(-x_1, -x_2) = -u_1(x_1, x_2), \quad u_2(-x_1, -x_2) = -u_2(x_1, x_2). \tag{4}$$

One additional relevant condition for this case of loading is obtained through equilibrium considerations in the x_2 direction and is stated as

$$-\int_{AB} T_2 \, ds + \int_{EF} T_2 \, ds = \frac{3b}{2}\sigma_\infty \tag{5}$$

where T_2 is the traction component in the x_2 direction on the external boundaries AB and EF. This condition allows for the numerical determination of the remote applied stress σ_∞.

2.2. *Constitutive relations*

Now that the relevant conditions that must be satisfied on the external boundaries of the trapezoidal region ABEF have been given, we turn our attention to the individual material phases comprising the interior of the trapezoidal region. In the present analysis, a graphite/epoxy composite material system is considered, and a description of the constitutive law which governs the behavior of each phase follows.

Epoxy matrix and graphite fiber phases. It is assumed that the matrix is isotropic and linearly elastic. The fibers are taken to be linearly elastic and transversely isotropic. The elastic constants employed in this analysis were obtained by Kriz and Stinchcomb (1979) and are given in Table 1. For the case of plane strain, the stress–strain relations for the matrix phase can be written as

$$\varepsilon_{33} = \varepsilon_{13} = \varepsilon_{23} = 0$$
$$\sigma_{13} = \sigma_{23} = 0$$
$$\sigma_{33} = \lambda(\varepsilon_{11} + \varepsilon_{22})$$
$$\sigma_{\alpha\beta} = 2\mu\varepsilon_{\alpha\beta} + \lambda\varepsilon_{\gamma\gamma}\delta_{\alpha\beta} \tag{6}$$

where the parameters λ and μ are Lamé's constants and the Greek indices α, β and γ range over 1 and 2. For the transversely isotropic fiber phase, the elastic stress-strain relations for the case of plane strain are given by Hashin (1979). The non-zero components are written as

$$\sigma_{33} = l(\varepsilon_{11} + \varepsilon_{22})$$
$$\sigma_{\alpha\beta} = (K_T - G_T)\varepsilon_{\gamma\gamma}\delta_{\alpha\beta} + 2G_T\varepsilon_{\alpha\beta} \tag{7}$$

where the constant l is related to the axial Poisson's ratio ν_A and the transverse bulk modulus K_T by

$$l = 2K_T\nu_A. \tag{8}$$

In addition, the transverse bulk modulus K_T is related to the engineering constants by the relation

$$K_T = \frac{E_T E_A G_T}{4G_T E_A - E_T E_A - 4E_T G_T \nu_A^2} \tag{9}$$

where E_T and E_A are the transverse and axial Young's moduli of the fiber and G_T is the transverse shear modulus.

Interface model. Both a linearly elastic and a linearly viscoelastic constitutive relation are considered for the interfacial zone. For the linearly elastic interface, it is assumed that the normal traction between the fiber and matrix phases is proportional to the jump in the normal displacement across the interface. Similarly, the tangential traction is taken to be proportional to the jump in the tangential displacement across the interface. Thus,

$$\mathbf{T}_n = k_n[\mathbf{u}_n]_I$$
$$\mathbf{T}_t = k_t[\mathbf{u}_t]_I \tag{10}$$

where

$$\mathbf{u}_n = u_i n_i \mathbf{n} \quad \text{and} \quad \mathbf{T}_n = (\sigma_{ij} n_i n_j)\mathbf{n}$$
$$\mathbf{u}_t = \mathbf{u} - \mathbf{u}_n \quad \text{and} \quad \mathbf{T}_t = \mathbf{T} - \mathbf{T}_n \tag{11}$$

are the normal and tangential displacement and traction vectors respectively, $[\,.\,]_I$ denotes the jump in the relative quantity across the interface, k_n and k_t are normal and tangential stiffness parameters arbitrarily taken to be equal in this analysis, and $\mathbf{T}$ is the traction vector ($T_i = \sigma_{ij}n_j$). Here $\sigma_{ij} = \sigma_{ji}$ is the Cauchy stress tensor. A positive jump in normal displacement, $[\mathbf{u}_n]_I$, denotes normal separation between the fiber and matrix phases. However, we assume that a negative jump in normal displacement would correspond to a physically unrealistic interpenetration of the matrix phase into the fiber phase, and thus we enforce the impenetrability constraint

$$[\mathbf{u}_n]_t \geqslant 0. \tag{12}$$

For a linearly viscoelastic interface, the time-dependent response of the interfacial zone is taken into account. The material response in both the normal and tangential directions is considered to be that of a standard linear solid (SLS). The SLS qualitatively represents the behavior of an idealized cross-linked polymer and can be viewed as a spring in parallel with a spring and a dashpot. The normal and tangential tractions $\mathbf{T}_n$ and $\mathbf{T}_t$ are then related to the displacement jumps $[\mathbf{u}_n]_t$ and $[\mathbf{u}_t]_t$ across the interface by

$$\begin{aligned} \dot{\mathbf{T}}_n + \frac{\mathbf{T}_n}{\tau} &= k_{g_n}[\dot{\mathbf{u}}_n]_t + \frac{k_{\infty_n}}{\tau}[\mathbf{u}_n]_t \\ \dot{\mathbf{T}}_t + \frac{\mathbf{T}_t}{\tau} &= k_{g_t}[\dot{\mathbf{u}}_t]_t + \frac{k_{\infty_t}}{\tau}[\mathbf{u}_t]_t \end{aligned} \tag{13}$$

where k_{g_n} and k_{g_t} are the instantaneous (glassy) stiffness components and k_{∞_n} and k_{∞_t} are the long-term (rubbery) stiffness components of the SLS. For convenience, the time constant τ in expression (13) is taken to be unity throughout.

3. FINITE ELEMENT IMPLEMENTATION

In order to solve the now formulated boundary value problem, the finite element method is employed. Throughout, we assume small displacements. The strain displacement relation then takes the usual form

$$\varepsilon_{ij} = (u_{i,j} + u_{j,i})/2 \tag{14}$$

and the equilibrium equation is written as

$$\sigma_{ij,j} = 0. \tag{15}$$

For a fiber-reinforced composite with an interfacial zone, the Principle of Virtual Work is written as

$$\int_\Omega \sigma_{ij}\delta\varepsilon_{ij}\,\mathrm{d}\Omega + \int_S \delta\phi\,\mathrm{d}S = \int_\Gamma T_i\delta u_i\,\mathrm{d}\Gamma \tag{16}$$

where Ω denotes the interior of the trapezoidal region shown in Fig. 2, Γ is the external traction boundary, and S is the interfacial traction boundary. The δu_i are the kinematically admissible displacements (satisfying the periodic displacement boundary conditions outlined in Section 2 and vanishing on the prescribed displacement boundary). The second term in (16) is the virtual work of separation of the matrix and fiber phases, i.e.

$$\delta\phi = T_n\delta[u_n]_t + T_t\delta[u_t]_t. \tag{17}$$

The stiffness contribution of the interfacial zone arises naturally from this expression. A four-node interface element with no thickness in its undeformed configuration is employed in the numerical calculations. A brief formulation of the stiffness matrix for a single interface element is given in Appendix B. Note that for the case of a linearly viscoelastic interface, the time dependence of the interface enters into the formulation, and (16) must be discretized in both space and time. A detailed formulation of this discretization is found in Appendix C.

In order to approximately satisfy the impenetrability constraint (12), full Newton Raphson equilibrium iteration is employed with a penalty-like stress update scheme in which the interface is taken to have a suitably high normal stiffness parameter in compression.

4. MACROSCOPIC BEHAVIOR

The numerical results of the present analysis provide a direct method for calculating the effective transverse properties of the fiber-reinforced composite. For a composite with a linearly elastic interface, the numerical results for the effective transverse bulk and shear moduli are compared with the results of Hashin (1990), where the composite cylinder assemblage (CCA) model is employed to obtain the effective transverse bulk modulus, and the generalized self-consistent scheme (GSCS) model is used to determine the effective transverse shear modulus. It is noted that the CCA model has been introduced in Hashin and Rosen (1964) and generalized to transversely isotropic fibers and matrix in Hashin (1979). In the context of perfect interface conditions the GSCS model has been applied by Christensen and Lo (1979) to obtain the transverse shear modulus. For a linearly viscoelastic interface, the numerical results are compared with approximate expressions derived analytically for the time-dependent transverse properties of the composite.

4.1. *Linearly elastic fiber/matrix interface*

It can be shown analytically that, due to its inherent elastic symmetry, the hexagonal array composite with linearly elastic constituents is transversely isotropic, see Love (1927) and Lekhnitskii (1963). Therefore, we assume that the effective elastic moduli C^*_{ijkl} are related to the Cartesian components of the macroscopic or average stress and strain tensors $\bar{\sigma}_{ij}$ and $\bar{\varepsilon}_{ij}$ in the form

$$\bar{\sigma}_{ij} = C^*_{ijkl}\bar{\varepsilon}_{kl} \tag{18}$$

and that this relation takes the form (7) where the quantities in each expression are replaced by their respective averaged or macroscopic counterparts (e.g. $\bar{\varepsilon}_{11}$ is substituted for ε_{11}, K^*_1 for K_1 etc.). The macroscopic response of the composite is significantly influenced by the impenetrability condition (12), which acts as a unilateral constraint on the deformation of the interface. When the constraint is not imposed, the response is tranversely isotropic as expected. When the constraint is imposed, the response is not transversely isotropic but depends upon the direction and character of the loading. For example, the constraint gives rise to significant differences in the tensile and compressive response. These differences are most pronounced when the interfacial stiffness parameters are low. In the present investigation we consider uniaxial tensile loading only, and in this case the deviations from transverse isotropy are slight.

Numerical procedure. Under the condition of CPD loading, the effective transverse shear and bulk moduli of the composite are obtained in the following manner. First, a constant displacement Δ_2 is applied along the external boundary EF, and a constant displacement $-\Delta_2$ is applied along the external boundary AB (see Fig. 2). The solution of the finite element equations yields the unknown, constant displacement Δ_1 along the external boundary AF. The average strain in the x_1 direction is then given by

$$\bar{\varepsilon}_{11} = \frac{-4\Delta_1}{3b}. \tag{19}$$

The average strain in the x_2 direction is given by

$$\bar{\varepsilon}_{22} = \frac{4}{\sqrt{3}}\frac{\Delta_2}{b}. \tag{20}$$

By employing relation (5), the finite element solution also yields the remote applied stress. This is equal to the average stress component $\bar{\sigma}_{22}$ of the composite. Since there is no applied loading in the x_1 direction, the average stress component $\bar{\sigma}_{11} = 0$. Finally, by substituting these averaged quantities into the plane strain constitutive relation (7), the effective transverse shear and bulk moduli are found to be

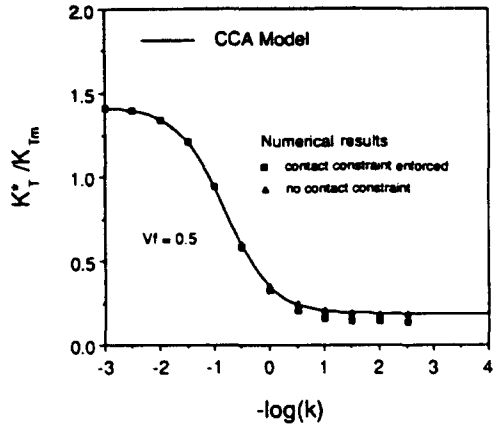

Fig. 3. Normalized effective transverse bulk modulus versus interface stiffness.

$$G_T^* = \frac{\bar{\sigma}_{22}}{2(\bar{\varepsilon}_{22} - \bar{\varepsilon}_{11})} \tag{21}$$

$$K_T^* = \frac{\bar{\sigma}_{22}}{2(\bar{\varepsilon}_{22} + \bar{\varepsilon}_{11})}. \tag{22}$$

Effective transverse bulk modulus. The numerical results for the effective transverse bulk modulus K_T^* are compared with the results of Hashin (1990), where the CCA model is employed. The CCA expression is given as

$$K_T^* = K_{T_m} + \frac{V_f}{\dfrac{1}{\bar{K}_{T_f} - K_{T_m}} + \dfrac{V_m}{K_{T_m} + G_{T_m}}} \tag{23}$$

where K_{T_m} and G_{T_m} are the transverse bulk and shear moduli of the matrix, and V_m and V_f are the matrix and fiber volume fractions. The quantity $\bar{K}_{T_f}$ is the equivalent transverse bulk modulus of the fiber–interface combination and can be expressed as

$$\bar{K}_{T_f} = \frac{aK_{T_f}k_n}{ak_n + 2K_{T_f}} \tag{24}$$

where k_n is the normal interfacial stiffness parameter, K_{T_f} is the transverse bulk modulus of the fiber, and a is the fiber radius. The numerical and CCA results for the effective transverse bulk modulus are shown in Fig. 3. The effective modulus K_T^* is plotted versus the normalized interfacial stiffness. The normalization is chosen such that

$$k = \frac{k_n}{G_{T_m}/a} \tag{25}$$

where a is the radius of the fiber. As expected, when the impenetrability constraint (12) is not enforced, the numerical and CCA results virtually coincide over the entire range of interface stiffness parameters. However, when this constraint is enforced, the numerical results deviate from the CCA results at relatively low interfacial stiffness parameters. The magnitude of this deviation depends on the loading condition considered in the numerical procedure. It is recalled that in the present analysis K_T^* is determined by subjecting the hexagonal array model to tensile uniaxial loading. It is noted that when condition (12) is not imposed, the numerical value obtained for K_T^* is independent of the loading condition considered.

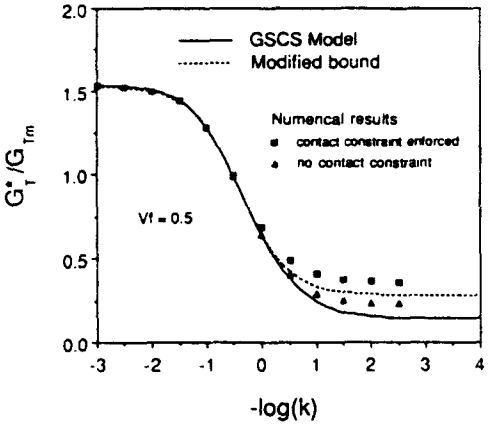

Fig. 4. Normalized effective transverse shear modulus versus interface stiffness.

Effective transverse shear modulus. As pointed out by Hashin (1990), the effective transverse shear modulus cannot in general be determined by employing the equivalent fiber–interface concept. Unlike the CCA expression for the effective transverse bulk modulus which is completely independent of the tangential interface stiffness parameter, the effective transverse shear modulus is highly dependent on both stiffness components. However, for the case when both the normal and tangential stiffness parameters are taken to be equal, it is found that the expression for the effective transverse shear modulus obtained by substituting approximate models for the fiber–interface shear modulus into available perfect interface expressions serves as a good approximation over a large range of interfacial stiffness values.

In the present analysis, we employ an approximate expression for the shear modulus of the fiber interface combination which is written as

$$\bar{G}_{T_f} = \frac{aG_{T_f}k_t}{ak_t + 2G_{T_f}} \tag{26}$$

where k_t is the tangential interfacial stiffness parameter, G_{T_f} is the transverse shear modulus of the fiber phase, and a is the fiber radius. It is noted that when the normal and tangential stiffness parameters are taken to be equal, the result obtained by substituting (26) for the transverse shear modulus of the fiber in the expression of Christensen and Lo (1979) is indistinguishable from the GSCS result of Hashin (1990). In Fig. 4, the GSCS results obtained by Hashin (1990) are compared with the numerical results. Results obtained by substituting (26) for the shear modulus of the fiber phase in the lower bound expression for arbitrary phase geometry given by Hashin (1979) are also shown in the figure. The effective transverse shear modulus normalized with respect to the shear modulus of the matrix is plotted versus normalized interfacial stiffness. Again, the normalization is chosen as in (25). When the impenetrability constraint (12) is enforced, the numerical results deviate significantly from the GSCS results at relatively low interfacial stiffness parameters. When constraint (12) is not enforced, the deviation at low stiffnesses is less significant. Again, when (12) is enforced, the magnitude of the deviation depends on the loading condition imposed on the hexagonal array model in the numerical procedure. It is noticed that under these circumstances the modified bound expression serves as a good model for the effective transverse shear modulus of the composite. It must be remembered, however, that this modified bound expression is not a bound but an approximate model for the effective transverse shear modulus. The corresponding results for the effective transverse bulk and shear modulus versus fiber volume fraction for a fixed normalized interfacial stiffness parameter ($k = 0.1$) are shown in Fig. 5.

4.2. *Linearly viscoelastic fiber/matrix interface*

In principle, if expressions for the effective moduli of the composite with a linearly elastic interface are known, the correspondence principle can be employed in order to

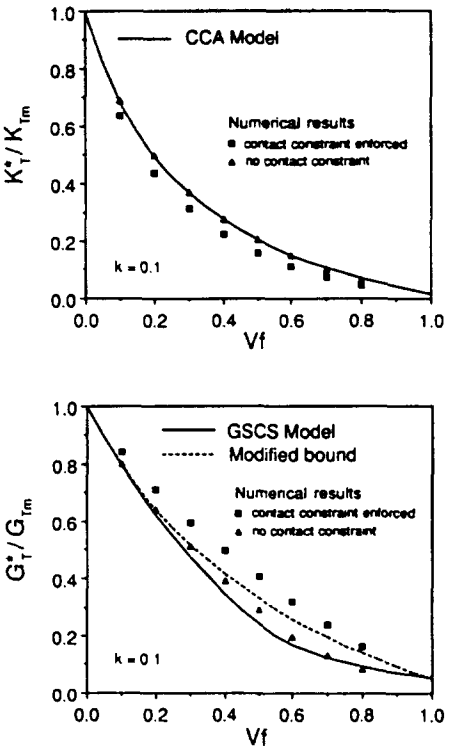

Fig. 5. Normalized transverse bulk and shear moduli versus fiber volume fraction.

calculate the effective time-dependent expressions for the composite with a linearly viscoelastic interface. Unfortunately, the exact elastic expression for the composite under consideration remains to be determined. However, it is noticed that the CCA results for the effective transverse bulk modulus given in the previous section compare closely with the numerical results for a wide range of stiffness parameters over the entire range of volume fractions considered. We thus choose the linearly elastic CCA expression and employ the correspondence principle to obtain a model for the time-dependent effective modulus $K_T^*(t)$ of the fiber-reinforced composite with a linearly viscoelastic interfacial zone. In order to obtain an analytic expression for the time-dependent effective transverse shear modulus $G_T^*(t)$, the modified bound expression obtained in the previous section is chosen since it is algebraically simple and lends itself well to analytic Laplace transform inversion. However, it is noted that the usefulness of the resulting time-dependent model for the effective transverse shear modulus is limited, since it is only valid for the special case when the normal and tangential interfacial stiffness parameters are assumed to be synchronous during interfacial stress relaxation.

Analytical model. By substituting the transformed relaxation function of the SLS, $sG(s)$, into (24) and (26), the transformed expressions $s\bar{K}_{T_f}(s)$ and $s\bar{G}_{T_f}(s)$ are obtained. Substitution of these expressions for $\bar{K}_{T_f}$ and $\bar{G}_{T_f}$ in the CCA result (23) and the lower bound result of Hashin (1979) yields $sK_T^*(s)$ and $sG_T^*(s)$. Generally a problem arises here in inverting back into the time domain. However, for this relatively simple viscoelastic interface model, the relations for $K_T^*(s)$ and $G_T^*(s)$ are easily inverted, yielding a model for the time-dependent effective moduli $K_T^*(t)$ and $G_T^*(t)$. The effective relaxation function in bulk can be expressed as

$$K_T^*(t) = K_{T_\infty}^* + (K_{T_0}^* - K_{T_\infty}^*)\,e^{-t/T_K} \tag{27}$$

while the effective relaxation function in shear can be written as

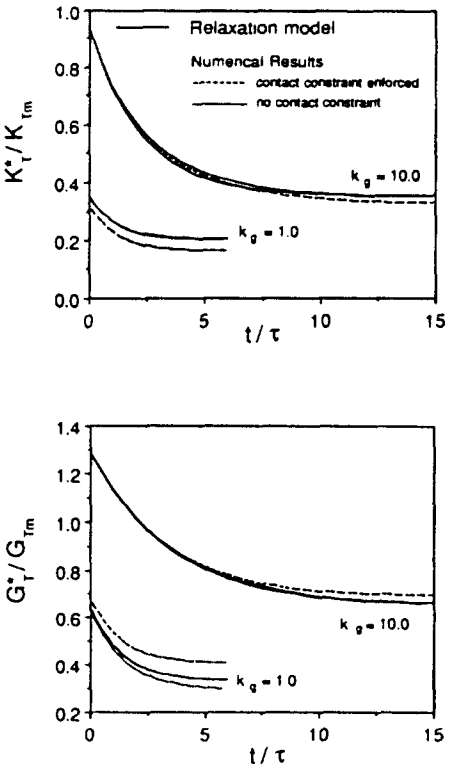

Fig. 6. Comparison of relaxation model in transverse bulk and shear with the numerical results (linearly viscoelastic interfacial zone).

$$G_T^*(t) = G_{T_\infty}^* + (G_{T_g}^* - G_{T_\infty}^*)\,e^{-t/T_G} \tag{28}$$

where $K_{T_g}^*$ and $G_{T_g}^*$ are the glassy or instantaneous values for the effective transverse shear and bulk moduli of the composite, $K_{T_\infty}^*$ and $G_{T_\infty}^*$ are the corresponding long-term values obtained as time approaches infinity, and T_K and T_G are the respective time constants in transverse bulk and shear. These quantities are defined in Appendix A.

Comparison of analytical model with numerical results. The numerical procedure employed to determine the effective relaxation moduli $K_T^*(t)$ and $G_T^*(t)$ is almost identical to that used in the numerical determination of the elastic transverse moduli. A step displacement $\Delta_2 H(t)$ is applied along the external boundary EF, and $-\Delta_2 H(t)$ is applied along the external boundary AB (see Fig. 2). Using relations (21) and (22), the effective moduli are computed and plotted as a function of time. The effective relaxation moduli $K_T^*(t)$ and $G_T^*(t)$ predicted by the analytical model and those obtained numerically are plotted for a fixed fiber volume fraction ($V_f = 0.5$) as shown in Fig. 6. Again, the normal and tangential interfacial stiffness parameters are assumed to be synchronous during interfacial stress relaxation, and the glassy stiffness of the interface ranges from a normalized value of ($k_g = 10$) to a normalized value of ($k_g = 1$). Throughout, the ratio of glassy to long-term interfacial stiffness is taken to be ($k_g/k_\infty = 10$). The normalization is chosen such that

$$k_g = \frac{k_{g_n}}{G_{T_m}/a}$$

$$k_\infty = \frac{k_{\infty_n}}{G_{T_m}/a}. \tag{29}$$

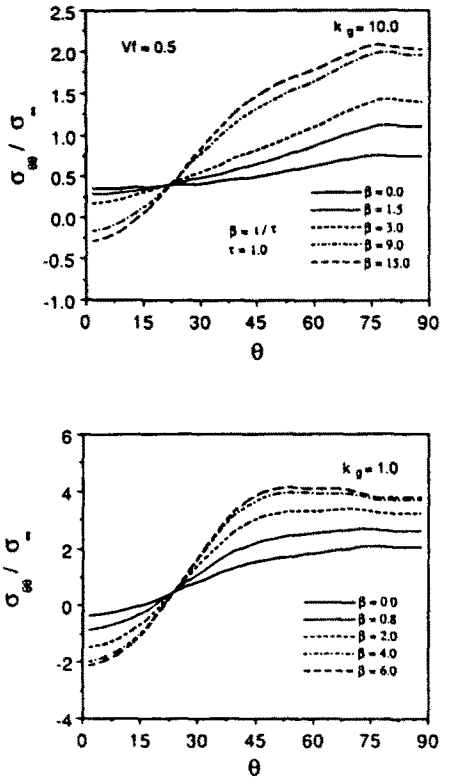

Fig. 7. Normalized hoop stress distributions in the matrix material just outside the interface during stress relaxation.

As shown in the figure, the approximate analytical model compares extremely well with the numerical results over the range where the interfacial stiffness is relatively high. As expected, when constraint (12) is enforced, for the relatively low glassy stiffness value ($k_g = 1$), the numerical results lie below the derived results for the transverse bulk relaxation modulus, and above the derived results for the transverse shear relaxation modulus. It is interesting to note that when the impenetrability constraint (12) is relaxed, the numerical results virtually coincide with the model over the entire range.

5. MICROSCOPIC BEHAVIOR

In this section, we turn from a macroscopic perspective and focus on the local or microscopic behavior of the transversely-loaded fiber-reinforced composite. In particular, we examine the influence of interfacial stress relaxation on the stress fields in the matrix material contiguous to the interface. Throughout, the composite is subjected to a step displacement in the mid-CPD loading direction, the more severe of the two loading cases considered, and normalized circumferential stress distributions in the matrix material just outside of the interface are obtained during the numerical simulation of stress relaxation.

During the interfacial stress relaxation, the circumferential stress $\sigma_{(m)}$ normalized with respect to the remote applied stress σ_∞ is plotted versus angle θ as shown in Fig. 7. In the upper diagram, the normalized glassy stiffness of the interface is taken to be ($k_g = 10$), and the ratio of glassy to long-term stiffness is taken to be ($k_g/k_\infty = 10$). Again, the time constant τ is taken to be unity for convenience. As shown in the figure, the normalized circumferential stress increases substantially as time progresses and as the effective stiffness of the interface decreases. Note that as the interface relaxes, a relatively abrupt change in the distributions occurs at approximately 75°. This is due to a local stress concentration at the transitional point where the compressive region of the interface begins. The resulting distributions, as interfacial stress relaxation proceeds, are shown in the lower diagram where the normalized

glassy stiffness of the interface is taken to be ($k_g = 1$). As time progresses, a noticeable shift occurs in the distributions. The maximum normalized circumferential stress gradually relocates from approximately 75° to approximately the 45° mark. In a recent experimental study by Daniel *et al.* (1989), when a silicon carbide/glass–ceramic composite having closely spaced, near hexagonally packed fibers was transversely loaded, fracture was observed to initiate in the form of radial cracks in the matrix at this 45° location.

6. CONCLUDING REMARKS

In the present work, the transverse loading of the hexagonal array composite is examined from both a macroscopic and a microscopic point of view. In the macroscopic analysis, the composite is subjected to tensile loading and the effective transverse properties are obtained. For the case of a linearly elastic interface, the numerical results are compared with expressions obtained from the composite cylinder assemblage and generalized self-consistent scheme models. It is found that when the impenetrability constraint is imposed, the mechanical behavior of the hexagonal array composite deviates slightly from transverse isotropy and the numerical results deviate significantly from the analytic expressions at low interfacial stiffness values. The magnitude of this deviation depends on the loading configuration considered in the numerical procedure. Note that we impose this constraint to avoid an unrealistic interpenetration of the matrix phase into the fiber phase. For the case of a linearly viscoelastic interface, the numerical results for the time-dependent transverse moduli are compared with approximate expressions derived analytically. Good agreement is found among the results over a large range of interfacial stiffnesses. In the micromechanical analysis, normalized circumferential stress distributions are obtained in the matrix material contiguous to the interface during interfacial stress relaxation. It is found that these distributions change substantially as the effective stiffness of the interface decreases. The maximum circumferential stress concentration is found to occur at approximately 45° at relatively low interfacial stiffness values.

Acknowledgements—This work was carried out in the course of research sponsored by the U.S. Navy (Contract No. N00014-86-K-0799) under Subcontract No. 89-122 to Northwestern University. Helpful discussions with Professor Z. Hashin, Dr Han Zhu and Professor I. M. Daniel are gratefully acknowledged.

REFERENCES

Aboudi, J. (1987). Damage in composites—modeling of imperfect bonding. *Comp. Sci. Technol.* **28**, 102–128.

Achenbach, J. D. and Zhu, H. (1989a). Effect of interfacial zone on mechanical behavior and failure of fiber-reinforced composites. *J. Mech. Phys. Solids* **37**, 381–393.

Achenbach, J. D. and Zhu, H. (1989b). Effect of interphases on micro- and macro-mechanical behavior of hexagonal array fiber composites. To be published in *J. Appl. Mech.*

Christensen, R. M. and Lo, K. H. (1979). Solutions for effective shear properties in three phase sphere and cylinder models. *J. Mech. Phys. Solids* **27**, 315–330.

Daniel, I. M., Anastassopoulos, G. and Lee, J. W. (1989). Failure mechanisms in ceramic matrix composites. *Proc. 1989 SEM Spring Conf. on Experimental Mechanics*, Cambridge, MA, pp. 832–838.

Hashin, Z. (1979). Analysis of properties of fiber composites with anisotropic constituents. *J. Appl. Mech.* **46**, 543–550.

Hashin, Z. (1990). Thermoelastic properties of fiber composites with imperfect interface. *Mech. Mater.* **8**, 333–348.

Hashin, Z. and Rosen, B. W. (1964). The elastic moduli of fiber reinforced materials. *J. Appl. Mech.* **31E**, 223–232.

Kriz, R. D. and Stinchomb, W. W. (1979). Elastic moduli of transversely isotropic graphite fibers and their composites. *Exp. Mech.* **19**, 41–49.

Lekhnitskii, S. G. (1963). *Theory of Elasticity of an Anisotropic Elastic Body*. Holden-Day, San Francisco.

Love, A. E. H. (1927). *A Treatise on the Mathematical Theory of Elasticity*. Cambridge University Press, Cambridge.

Needleman, A. (1987). A continuum model for void nucleation by inclusion debonding. *J. Appl. Mech.* **54**, 525–531.

Steif, P. S. and Hoysan, S. F. (1987). An energy method for calculating the stiffness of aligned short-fiber composites. *Mech. Mater.* **6**, 197–210.

Taylor, R. L., Pister, K. S. and Goudreau, G. L. (1970). Thermomechanical analysis of viscoelastic solids. *Int. J. Numer. Meth. Engng* **2**, 45–59.

APPENDIX A: DEFINITIONS

In this Appendix, we define the quantities contained within the derived expressions (27) and (28) for the time-dependent relaxation moduli. The expressions for $K^*_{T_g}$ and $G^*_{T_g}$ are obtained by making the following substitutions:

(1) Substitute for k_n in (24) k_{g_n}, the glassy stiffness component of the SLS in the normal direction to obtain the intermediate expression $\bar{K}_{T_g}$ for the glassy effective bulk modulus of the fiber–interface combination. Similarly, substitute for k_t in (26) k_{g_t}, the glassy stiffness component of the SLS in the tangential direction to obtain the glassy effective shear modulus $\bar{G}_{T_g}$ of the fiber–interface combination.
(2) Substitute the expression $\bar{K}_{T_g}$ into the CCA result (23) and $\bar{G}_{T_g}$ into the lower bound expression for the arbitrary phase geometry of Hashin (1979).

Thus, the effective glassy moduli are written as

$$K^*_{T_g} = K_{T_m} + \frac{V_f}{\dfrac{1}{\bar{K}_{T_g} - K_{T_m}} + \dfrac{V_m}{K_{T_m} + G_{T_m}}} \tag{A1}$$

$$G^*_{T_g} = G_{T_m} + \frac{V_f}{\dfrac{1}{\bar{G}_{T_g} - G_{T_m}} + \dfrac{(K_{T_m} + 2G_{T_m})V_m}{2G_{T_m}(K_{T_m} + G_{T_m})}} \tag{A2}$$

where

$$\bar{K}_{T_g} = \frac{aK_{T_f}k_{g_n}}{ak_{g_n} + 2K_{T_f}} \tag{A3}$$

$$\bar{G}_{T_g} = \frac{aG_{T_f}k_{g_t}}{ak_{g_t} + 2G_{T_f}} \tag{A4}$$

and the long-term effective moduli are expressed as

$$K^*_{T_\infty} = K_{T_m} + \frac{V_f}{\dfrac{1}{\bar{K}_{T_\infty} - K_{T_m}} + \dfrac{V_m}{K_{T_m} + G_{T_m}}} \tag{A5}$$

$$G^*_{T_\infty} = G_{T_m} + \frac{V_f}{\dfrac{1}{\bar{G}_{T_\infty} - G_{T_m}} + \dfrac{(K_{T_m} + 2G_{T_m})V_m}{2G_{T_m}(K_{T_m} + G_{T_m})}} \tag{A6}$$

where

$$\bar{K}_{T_\infty} = \frac{aK_{T_f}k_{\infty_n}}{ak_{\infty_n} + 2K_{T_f}} \tag{A7}$$

$$\bar{G}_{T_\infty} = \frac{aG_{T_f}k_{\infty_t}}{ak_{\infty_t} + 2G_{T_f}}. \tag{A8}$$

Finally, the time constants T_K and T_G are written in terms of the time constant τ of the SLS as

$$T_K = \frac{k_{g_n}}{k_{\infty_n}}\tau\frac{\bar{K}_{T_\infty}}{\bar{K}_{T_g}}\frac{1 + m(\bar{K}_{T_g} - K_{T_m})}{1 + m(\bar{K}_{T_\infty} - K_{T_m})} \tag{A9}$$

$$T_G = \frac{k_{g_t}}{k_{\infty_t}}\tau\frac{\bar{G}_{T_\infty}}{\bar{G}_{T_g}}\frac{1 + n(\bar{G}_{T_g} - G_{T_m})}{1 + n(\bar{G}_{T_\infty} - K_{T_m})} \tag{A10}$$

where

$$m = \frac{V_m}{K_{T_m} + G_{T_m}} \tag{A11}$$

$$n = \frac{(K_{T_m} + 2G_{T_m})V_m}{2G_{T_m}(K_{T_m} + G_{T_m})}. \tag{A12}$$

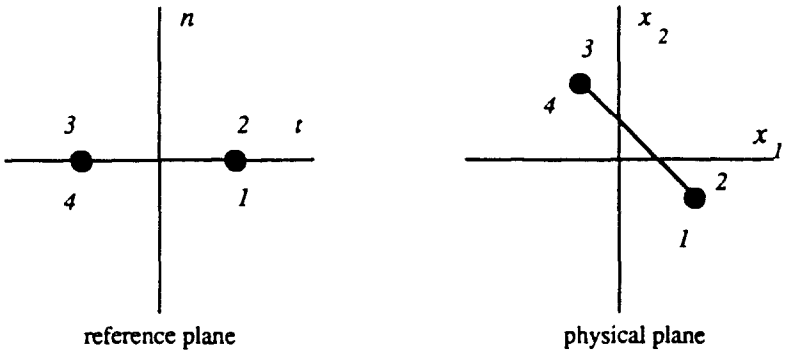

Fig. B1. Reference and physical plane representations of the 4-node interface element.

APPENDIX B: INTERFACE ELEMENT STIFFNESS FORMULATION

The following is a brief formulation of the stiffness matrix for a single interface element. Shown in Fig. B1 are the reference plane and physical plane representations of the 4-node interface element employed to model the interface layer between the fiber and matrix phases. As shown in the figure, nodes (1, 2) and nodes (3, 4) are coalesced, creating an interface element having no thickness in its undeformed state. The axes of the reference plane, n and t, correspond to directions normal and tangential to the interface boundary, while the axes of the physical plane, x_1 and x_2, correspond to the Cartesian coordinate system of Fig. 2. For a linearly elastic interface, the virtual work of separation of the matrix and fiber phases is written as

$$\delta\phi = k_n[u_n]_I\delta[u_n]_I + k_t[u_t]_I\delta[u_t]_I. \tag{B1}$$

It is assumed that the normal and tangential displacement jumps across the interface $[u_n]_I$ and $[u_t]_I$ vary linearly along the length l of the element. The interpolation for this element is then

$$\begin{aligned}[u_n]_I &= \Delta d_{ni} N_i \\ [u_t]_I &= \Delta d_{ti} N_i\end{aligned} \tag{B2}$$

where the repeated index i is summed over 1, 2 and

$$\begin{aligned}\Delta d_{n1} &= d_{n3} - d_{n4}, \quad \Delta d_{n2} = d_{n2} - d_{n1} \\ \Delta d_{t1} &= d_{t3} - d_{t4}, \quad \Delta d_{t2} = d_{t2} - d_{t1}\end{aligned} \tag{B3}$$

are the discrete relative nodal displacements in the normal and tangential directions, respectively. The shape functions N_i in (B2) are given by

$$N_i = \tfrac{1}{2}(1 + t_i t) \tag{B4}$$

where the t_i are the coordinates of nodes (3, 4) and (1, 2) in the reference plane. The relative displacement field across the interface is then written in discrete form as

$$[\mathbf{u}]_I = \mathbf{N}\Delta\mathbf{d}. \tag{B5}$$

The vector containing the relative nodal displacements $\Delta\mathbf{d}$ is related to the actual nodal displacements $\mathbf{d}_j^{\mathrm{T}} = (d_{xj}, d_{yj})$, where the subscript j takes on the nodal values 1–4, by

$$\Delta\mathbf{d} = \mathbf{H}\mathbf{T}\mathbf{d}. \tag{B6}$$

Here $\mathbf{H}$ is a 4×8 Boolean operator matrix and $\mathbf{T}$ is a 8×8 coordinate transformation matrix. The element stiffness matrix then takes the familiar form

$$\mathbf{K}_e = \int_{S_e} \mathbf{B}^{\mathrm{T}}\tilde{\mathbf{D}}\mathbf{B}\,\mathrm{d}S \tag{B7}$$

where

$$\mathbf{B} = \mathbf{N}\mathbf{H}\mathbf{T} \tag{B8}$$

is the matrix which operates on the actual nodal displacements yielding the normal and tangential displacement jumps across the interface, and $\tilde{\mathbf{D}}$ is the matrix containing the interface stiffness parameters.

APPENDIX C: FINITE ELEMENT FORMULATION FOR LINEARLY VISCOELASTIC INTERFACE

For the case of a linearly viscoelastic interface, the time dependence of the interface enters into the formulation, and the Principle of Virtual Work

$$\int_\Omega \sigma_{ij}\delta\varepsilon_{ij}\,d\Omega + \int_S \delta\phi\,dS = \int_\Gamma T_i\delta u_i\,d\Gamma \tag{C1}$$

must be discretized both in space and time. The following implementational details are based on a solution procedure that has been discussed by Taylor *et al.* (1970). Writing (C1) in incremental form at time t_{n+1} yields

$$\int_\Omega \Delta\sigma_{ij}\delta\varepsilon_{ij}\,d\Omega + \int_S \Delta T_i\delta[u_i]_t\,dS = \int_\Gamma \Delta T_i\delta u_i\,d\Gamma - \left[\int_\Omega \sigma_{ij}\delta\varepsilon_{ij}\,d\Omega + \int_S T_i\delta[u_i]_t\,dS - \int_\Gamma T_i\delta u_i\,d\Gamma\right]_n \tag{C2}$$

where $(\sigma_{ij})_{n+1} = (\sigma_{ij})_n + (\Delta\sigma_{ij})_n$ and $(T_i)_{n+1} = (T_i)_n + (\Delta T_i)_n$. Using (C2) as our starting point, we now express the components T_i of the interfacial traction vector in terms of the $[u_i]_t$ as follows. The standard linear solid can be viewed as comprising two Maxwell elements in parallel, one with an infinite time constant, τ. The governing differential equation for one Maxwell element is simply expressed as

$$\dot{T}_i^j + \frac{T_i^j}{\tau^j} = (k_i^j)[\dot{u}_i]_t \tag{C3}$$

where the superscript j refers to the jth Maxwell element of the SLS. For extension at a constant rate, $[\dot{u}_i]_t$, the exact solution of (C3) is

$$T_i^j(t) = (k_i^j)[\dot{u}_i]_t\tau^j[1-\exp(-t/\tau^j)]. \tag{C4}$$

Letting $(\Delta[u_i]_t)_n = ([u_i]_t)_{n+1} - ([u_i]_t)_n$ and $\Delta t = t_{n+1} - t_n$, the interfacial traction components T_i at time t_{n+1} are obtained by expressing (C4) in incremental form and summing the partial stresses. Thus

$$(T_i)_{n+1} = \sum_{j=1}^{2}\left[T_i^j\exp(-\Delta t/\tau^j) + k_i^j\Delta[u_i]_t h(\Delta t)\right]_n \tag{C5}$$

where

$$h(\Delta t) = \tau^j(1-\exp(-\Delta t/\tau^j))/\Delta t. \tag{C6}$$

Note that as the time constant τ^j approaches infinity, $h(\Delta t)$ in (C6) approaches unity. Referring back to eqn (C2), we introduce standard finite element shape functions, N, and use the arbitrariness of the variations in the nodal displacements to obtain the discrete form

$$\sum_{e=1}^{n_e}\left[\int_\Omega \mathbf{B}_e^{\mathrm{T}}\mathbf{D}_e\mathbf{B}_e\,d\Omega + \int_S \mathbf{B}^{\mathrm{T}}\tilde{\mathbf{D}}\mathbf{B}\,dS\right]_n \Delta\mathbf{d}_e^i = \sum_{e=1}^{n_e}\left[\int_\Gamma \mathbf{N}_e^{\mathrm{T}}\mathbf{T}_{n+1}^i\,d\Gamma - \int_S \mathbf{B}^{\mathrm{T}}\mathbf{T}_{n+1}^i\,dS - \int_\Omega \mathbf{B}_e^i\sigma_{n+1}^i\,d\Omega\right] \tag{C7}$$

where the vector $\Delta\mathbf{d}_e^i$ contains the discrete nodal displacement increments at the ith iteration and n_e refers to the number of elements in the model. The first term on the left side of (C7) contains the symmetric gradient operator matrix $\mathbf{B}_e$ and the plane strain constitutive matrix $\mathbf{D}_e$. The second term on the left side of (C7) constitutes the interface stiffness contribution of the interface layer; see Appendix B for interface element formulation. Here, the interface constitutive matrix, $\tilde{\mathbf{D}}$, is a 2×2 diagonal matrix whose components are given by

$$\begin{aligned}\tilde{D}_{11} &= \sum_{j=1}^{2} h(\Delta t)k_n^j\\ \tilde{D}_{22} &= \sum_{j=1}^{2} h(\Delta t)k_t^j\end{aligned} \tag{C8}$$

where k_n^j and k_t^j are the normal and tangential stiffness parameters associated with the jth Maxwell element of the SLS, and $h(\Delta t)$ is defined by (C6). Note that this entire procedure can easily be extended for more general constitutive relations, for example, by modeling the normal and tangential material response of the interface with a greater number of Maxwell elements.